Chapter 19
Collective Nuclear Excitations

We showed in Sect. 18.3 that the nuclear ground states may be well described if we assume that the nucleons are in the lowest shell-model orbits. The single-particle picture, we further showed for the case of a *single* valence nucleon or nucleon hole, works very well if shells are nearly full or empty. Excited states are then understood as being created by a valence nucleon jumping into a higher shell-model state; a direct analogy to our picture of the atom. As well as such straightforward single-particle excitations, more complicated phenomena can take place in the nucleus. Collective excitations provide some of the most beautiful aspects of nuclear dynamics.

Collective excitations of many-body systems can be phenomenologically understood as fluctuations around a state of equilibrium. These may be fluctuations in density or shape. The type of collective excitation strongly depends upon the composition of the system and the manner in which its components interact with each other. We want now to show the connection between nuclear collective excitations and the forces inside and the structure of the nucleus.

Electromagnetic transitions provide us with the most elegant way to investigate collective excitations in nuclei. We will therefore first consider how electromagnetic transitions in nuclei may be determined, so that we can then say to what extent collective effects are responsible for these transitions.

The first measurements of photon absorption in nuclei led to the discovery that the lion's share of the the absorption is by a *single* state. The first description of this *giant dipole resonance* state was of an oscillation of the protons and neutrons with respect to each other. Later on it was discovered that the transition probability for electric quadrupole transitions of lower energy states was much higher than a single-particle picture of the nucleus predicts. The transition probability for octupole transitions also predominantly stems from single states which we call octupole vibrations.

B. Povh et al., *Particles and Nuclei*, Graduate Texts in Physics,
DOI 10.1007/978-3-662-46321-5_19

The single-particle and collective properties of nuclei were regarded for a long time as distinct phenomena. A unified picture first appeared in the 1970s. We want to illustrate this modern framework through the example of giant dipole resonances. What we will discover can be easily extended to quadrupole and octupole oscillations.

Another important collective effect is the rotation of deformed nuclei. Such rotations form a most pleasing chapter, both didactically and aesthetically, in the story of γ spectroscopy.

19.1 Electromagnetic Transitions

Electric dipole transitions The probability of an electric dipole transition can be somewhat simplistically derived by considering a classical Hertz dipole. The power output emitted by the dipole is proportional to ω^4. The rate of photon emission, i.e., the transition probability, may be obtained by dividing the power output by the photon energy $\hbar\omega$. One so finds

$$W_{fi} = \frac{1}{\tau} = \frac{e^2}{3\pi\varepsilon_0\hbar^4 c^3} E_\gamma^3 \left| \int \mathrm{d}^3x \; \psi_f^* \boldsymbol{x} \psi_i \right|^2 , \tag{19.1}$$

where we have replaced the classical dipole $e\boldsymbol{x}$ by the matrix element. This result may also be obtained directly from quantum mechanics.

■ In the following derivation we want to treat the electromagnetic transitions semiclassically, i.e., we will not concern ourselves with quantising the radiation field or spin.

Consider first an excited nuclear state ψ_i which through γ emission enters a lower lying state, ψ_f. The golden rule says that the transition probability is

$$\mathrm{d}W = \frac{2\pi}{\hbar} \, |\langle \psi_f | \mathcal{H}_{\mathrm{int}} | \psi_i \rangle|^2 \, \mathrm{d}\varrho(E) \, . \tag{19.2}$$

$\mathcal{H}_{\mathrm{int}}$ describes the interaction of the moving charge with the electromagnetic field and $\varrho(E)$ is a phase space factor that describes the final state density at total energy E. For photon emission we have $E = E_\gamma$. Since γ radiation is generally not spherically symmetric, we consider the phase space in a solid angle element $\mathrm{d}\Omega$ around the momentum vector. As in (4.16) we set

$$\mathrm{d}\varrho(E) = \frac{V \, |\boldsymbol{p}|^2 \, \mathrm{d}|\boldsymbol{p}| \, \mathrm{d}\Omega}{(2\pi\hbar)^3 \, \mathrm{d}E} \, . \tag{19.3}$$

For the photon we have $E = c|\boldsymbol{p}|$ and $\mathrm{d}E = c\mathrm{d}|\boldsymbol{p}|$, which implies

$$\mathrm{d}\varrho(E) = \frac{E_\gamma^2 \, V \, \mathrm{d}\Omega}{(2\pi\hbar c)^3} \, . \tag{19.4}$$

The $\mathcal{H}_{\text{int}}$ operator can be obtained by considering the classical Hamiltonian for the interaction between a charge e, which emits the photon, and the electromagnetic field $A = (\phi/c, \boldsymbol{A})$ [10]:

$$\mathcal{H} = \frac{1}{2m}\,(\boldsymbol{p} - e\boldsymbol{A})^2 + e\phi\,. \tag{19.5}$$

Note that we have here assumed a point-like charge. The term quadratic in A is negligible and we may write

$$\mathcal{H} = \frac{\boldsymbol{p}^2}{2m} - \frac{e}{m}\boldsymbol{p}\boldsymbol{A} + e\phi\,. \tag{19.6}$$

The first term corresponds to free movement of the charged particle and the last two describe the interaction

$$\mathcal{H}_{\text{int}} = -\frac{e}{m}\boldsymbol{p}\boldsymbol{A} + e\phi\,, \tag{19.7}$$

which, for a point-like particle, is just given by the scalar product of the electric four-current

$$j = (e \cdot c, e\boldsymbol{v}) \tag{19.8}$$

and the electromagnetic field

$$A = (\phi/c, \boldsymbol{A})\,. \tag{19.9}$$

In an electromagnetic decay $e\phi$ does not contribute to the transition probability, since real photons are transversely polarised and monopole transitions are hence forbidden.

If one replaces the momentum $\boldsymbol{p}$ by the operator $\boldsymbol{p} = -i\hbar\nabla$ and interprets the vector $\boldsymbol{A}$ as the wave function of the photon, one obtains the matrix element

$$\langle\psi_f|\mathcal{H}_{\text{int}}|\psi_i\rangle = -\frac{ie\hbar}{m}\int \mathrm{d}^3x\;\psi_f^*\;\left(\nabla\psi_i\right)\boldsymbol{A}\,. \tag{19.10}$$

The gradient ∇ may be replaced by the commutator of the coordinate $\boldsymbol{x}$ with the Hamilton operator, since for stationary states

$$\mathcal{H}_0 = \frac{\boldsymbol{p}^2}{2m} + V(\boldsymbol{x}) \tag{19.11}$$

we have the following relation:

$$\boldsymbol{x}\,\mathcal{H}_0 - \mathcal{H}_0\,\boldsymbol{x} = \frac{i\hbar}{m}\boldsymbol{p} = \frac{\hbar^2}{m}\nabla\,. \tag{19.12}$$

In this way we have

$$-\frac{ie}{\hbar}\int \mathrm{d}^3x\;\psi_f^*\;(\boldsymbol{x}\mathcal{H}_0 - \mathcal{H}_0\boldsymbol{x})\;\psi_i\,\boldsymbol{A} \;=\; \frac{ie}{\hbar}(E_i - E_f)\int \mathrm{d}^3x\;\psi_f^*\,\boldsymbol{x}\,\psi_i\,\boldsymbol{A}\,, \tag{19.13}$$

and the matrix element has the standard form for multipole radiation.

In the semiclassical derivation of γ emission, one writes the photon wave function as

$$\boldsymbol{A} = \sqrt{\frac{\hbar}{2\varepsilon_0 \omega V}}\, \boldsymbol{\varepsilon} \cos(\boldsymbol{kx} - \omega t) \,, \tag{19.14}$$

where $\boldsymbol{\varepsilon}$ is the polarisation vector of the photon, $E_\gamma = \hbar\omega = E_i - E_f$ is its energy and $\boldsymbol{k}$ the wave vector. That this is indeed correct may be easily checked by calculating the electromagnetic radiation energy in a volume V using $\boldsymbol{A}$ from (19.14):

$$\hbar\omega = V \cdot \left(\frac{1}{2}\varepsilon_0 \overline{\boldsymbol{E}^2} + \frac{1}{2}\frac{1}{\mu_0}\overline{\boldsymbol{B}^2} \right) = V\varepsilon_0 \overline{\boldsymbol{E}^2} \qquad \text{with} \quad \boldsymbol{E} = -\frac{\partial \boldsymbol{A}}{\partial t} \,, \tag{19.15}$$

where the bar represents time averaging. With this result we now may write the transition probability as:

$$\begin{aligned} \mathrm{d}W_{fi} &= \frac{2\pi}{\hbar} \frac{\hbar}{2\varepsilon_0 \omega V} \frac{e^2 E_\gamma^2}{\hbar^2} \left| \boldsymbol{\varepsilon} \int \mathrm{d}^3x\, \psi_f^* \boldsymbol{x} \psi_i \; \mathrm{e}^{i\boldsymbol{kx}} \right|^2 \frac{E_\gamma^2\, V\, \mathrm{d}\Omega}{(2\pi\hbar c)^3} \\ &= \frac{e^2}{8\pi^2 \varepsilon_0 \hbar^4 c^3} E_\gamma^3 \left| \boldsymbol{\varepsilon} \int \mathrm{d}^3x\, \psi_f^* \boldsymbol{x}\, \mathrm{e}^{i\boldsymbol{kx}} \psi_i \right|^2 \mathrm{d}\Omega \,. \end{aligned} \tag{19.16}$$

The wavelengths of the gamma rays are large compared to a nuclear radius. The multipole expansion

$$\mathrm{e}^{i\boldsymbol{kx}} = 1 + i\boldsymbol{kx} + \ldots \tag{19.17}$$

is very useful, since, generally speaking, only the lowest transition that the quantum numbers allow needs to be taken into account. Only very occasionally are two multipoles of equal strength in a transition. If one now sets $\mathrm{e}^{i\boldsymbol{kx}} \approx 1$, integrates (19.16) over the solid angle $\mathrm{d}\Omega$ and the polarisation one obtains (19.1).

Electric dipole (E1) transitions always connect states with different parities. The photon carries away angular momentum $|\boldsymbol{\ell}| = 1\hbar$ and so the angular momenta of the initial and final states may at most differ by one unit.

Since transitions from one shell into the one immediately above play the most important role in collective excitations, we now introduce the standard notation for the wave function. A closed shell shall be denoted by the symbol $|0\rangle$ ("vacuum wave function"). If a particle in the state ϕ_{j_1} of the closed shell jumps into the state ϕ_{j_2} of the next shell a particle-hole state is created, which we symbolise by $|\phi_{j_1}^{-1}\phi_{j_2}\rangle$. The dipole matrix element

$$\langle \phi_{j_1}^{-1}\phi_{j_2} | e\boldsymbol{x} | 0 \rangle = e \int \mathrm{d}^3x\, \phi_{j_2}^* \boldsymbol{x} \phi_{j_1} \tag{19.18}$$

describes the transition of a nucleon from the state ϕ_{j_1} to the state ϕ_{j_2}. Since $|0\rangle$ is a full shell state it must have spin and parity $J^P = 0^+$, hence the excited particle-hole state after the electric dipole transition must have the quantum numbers $J^P = 1^-$.

Magnetic dipole transitions The transition probability of a magnetic dipole (M1) transition is obtained by replacing the electric dipole in (19.1) by a magnetic one:

$$W_{fi} = \frac{1}{\tau} = \frac{\mu_0}{3\pi\hbar^4 c^3} E_\gamma^3 \left| \int \mathrm{d}^3x \; \psi_f^* \boldsymbol{\mu} \psi_i \right|^2 , \qquad \text{where} \quad \boldsymbol{\mu} = \frac{e}{2m}(\boldsymbol{L} + g\boldsymbol{s}) . \tag{19.19}$$

Here $\boldsymbol{L}$ is the orbital angular momentum operator and $\boldsymbol{s}$ is the spin operator.

Higher multipoles If the electric dipole transition is forbidden, in other words if both states have the same parity or the vectorial addition of the angular momenta is inconsistent, then only higher multipole radiation can be emitted. The next highest multipoles in the transition probability hierarchy are the above magnetic dipole (M1) transition and the electric quadrupole (E2) transition [7]. Both are second order in the expansion (19.17). The parity of the initial and final states must be identical in electric quadrupole transitions and the triangle inequality $|j_f - j_i| \leq 2 \leq j_f + j_i$ must be fulfilled by the angular momenta. While the transition probability for dipole radiation is, from (19.1), proportional to E_γ^3, for electric quadrupole radiation it goes as E_γ^5. This is because there is a new factor of $i\boldsymbol{k}\boldsymbol{x}$ in the matrix element and $|\boldsymbol{k}|$ is proportional to E_γ. The energy-independent part of the matrix element has the form $r^2 Y_2^m(\theta, \varphi)$.

19.2 Dipole Oscillations

Photon absorption in nuclei A broad resonance, which was already known in the 1950s, dominates the absorption of gamma rays by nuclei. The experimental techniques for investigating this resonance were rather awkward since no variable energy gamma sources existed.

The method of in flight positron annihilation, which was developed in the 1960s, first permitted detailed measurements of the gamma cross-sections. Positrons, which have been produced through pair creation from a strong bremsstrahlung source, are selected according to their energy and focused upon a target. They then partially annihilate with the target electrons and produce bremsstrahlung as an unwanted by-product (Fig. 19.1).

Such a gamma spectrum is shown in Fig. 19.2. A peak can be clearly distinguished from the bremsstrahlung at the maximal possible energy and this is presumed to come from the e^+e^- annihilation. The energy dependence of γ-induced cross-sections can be thoroughly investigated by varying the energy of the positrons.

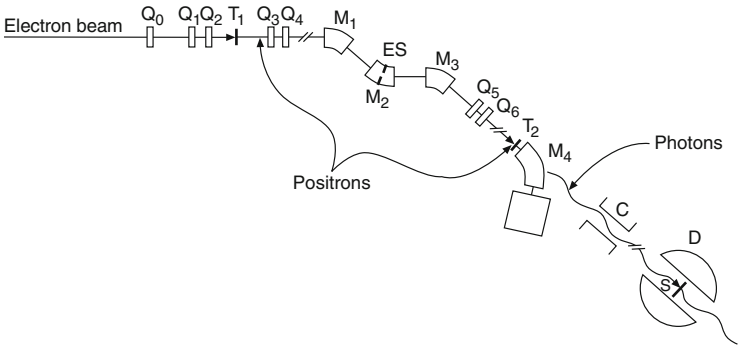

Fig. 19.1 Experimental set-up for in flight positron annihilation (From [2]). An electron beam hits a target (T_1). The bremsstrahlung that is produced converts into electron-positron pairs. The positrons are then selected according to their energy by three dipole magnets (M_1, M_2, M_3) before hitting a second target (T_2). Some of them annihilate in flight with target electrons. A further magnet (M_4) deflects all charged particles and only photons arrive at the experimenter's real target (S)

As well as the total cross-section, the cross-section for the photoproduction of neutrons (*nuclear photoeffect*)

$$^{A}\mathrm{X}\ (\gamma, \mathrm{n})\ ^{A-1}\mathrm{X} \tag{19.20}$$

is of special importance. This is in fact the major part of the total cross-section. The photoproduction of protons is, by contrast, suppressed by the Coulomb barrier. In what follows we will limit ourselves to the (γ, n) reaction.

We have chosen $\sigma(\gamma, \mathrm{n})$ for neodymium isotopes as an example (Fig. 19.3). Various observations may be made:

- The absorption probability is centred in a resonance which we call a *giant resonance*.
- The excitation energy of the giant resonance is roughly twice the separation between neighbouring shells. This is astounding since, for reasons of parity and angular momentum conservation, many more single-particle transitions are possible between one shell and the next than between a shell and the next but one.
- While a narrow resonance is observed in absorption by ^{142}Nd, this splits into two resonances as the mass number increases.
- The integrated cross-section is about as big as the sum over all expected cross-sections for the transition of a single nucleon from the last closed shell. This means that all the protons and neutrons of the outermost shell contribute coherently to this resonance.

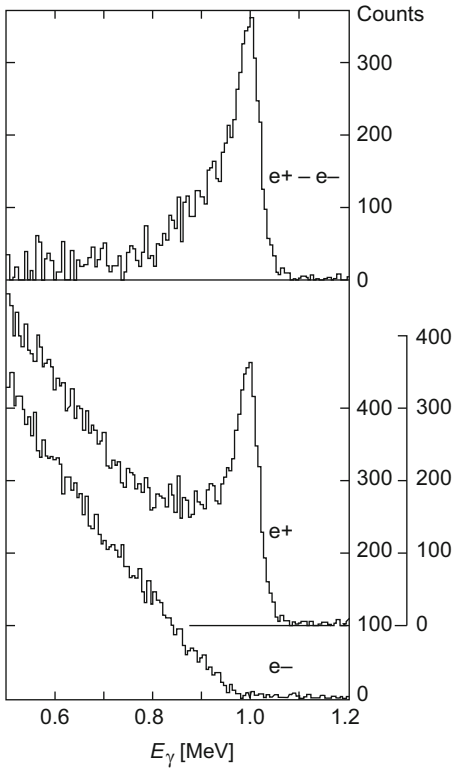

Fig. 19.2 The photon spectrum from in-flight electron positron annihilation [2]. This is later used for (γ, n) reactions. The background of bremsstrahlung from positrons hitting the target is determined by aiming a monoenergetic beam of electrons at the target. The cross-section for fixed photon energies is found by performing experiments with the two different photon beams and subtracting the counting rates

A qualitative explanation of the giant resonances comes from the oscillation of protons and neutrons with respect to each other (Fig. 19.4). The ^{150}Nd is deformed and has a cigar-like shape. The two maxima for this nucleus correspond to oscillations along the symmetry axis (lower peak) and orthogonal to it (higher peak).

We will attempt to justify this intuitive picture of giant resonances and their excitation energies in the framework of the shell model.

The giant dipole resonance Consider once again the example of the doubly magic ^{16}O nucleus. Let us assume that photon absorption leads to a nucleon in the $1p_{3/2}$ or $1p_{1/2}$ shell being excited into the $1d_{5/2}$, $1d_{3/2}$ or $2s_{1/2}$ shell. If this nucleon drops back into the 1p shell, it can pass on its excitation energy through recoils to other nucleons, which may then, for example, be themselves excited out of the 1p shell into the 1d or 2s shell. If the nuclear states that are produced by the excitation of a nucleon into a higher level were degenerate, then the probability of generating all of these states must be equal and a simple single-particle picture would be doomed to failure from the start. In reality this is almost the case; the excited states are almost degenerate.

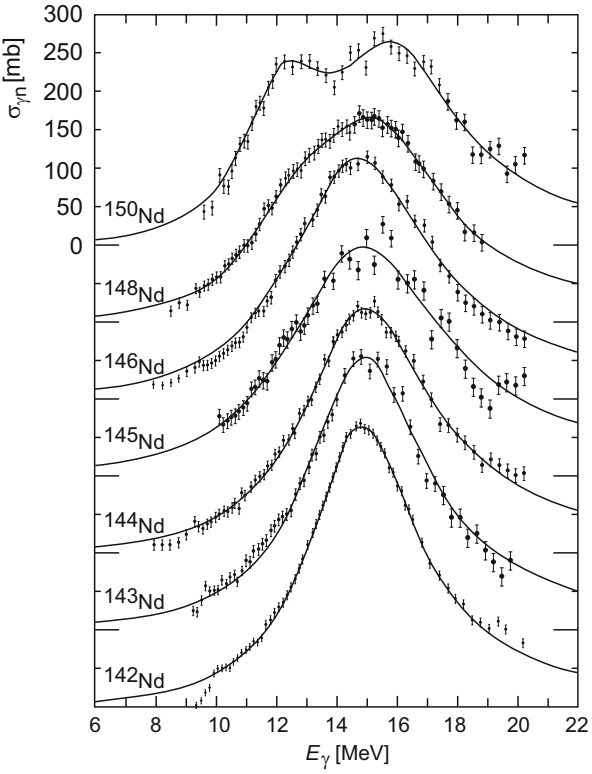

Fig. 19.3 Cross-section for γ-induced emission of neutrons in neodymium isotopes [2]. The curves have been shifted vertically for the sake of clarity. Neodymium isotopes progress from being spherically symmetric to being deformed nuclei. The giant resonance of the spherically symmetric ^{142}Nd nucleus is narrow, while that of the deformed ^{150}Nd nucleus shows a double peak

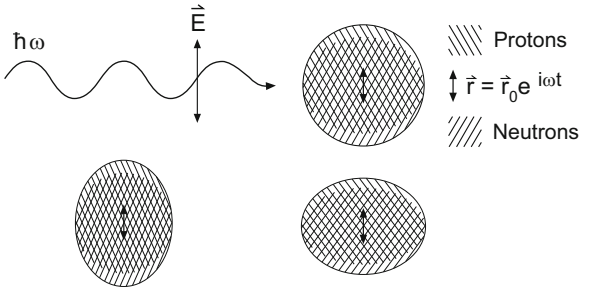

Fig. 19.4 The giant dipole resonance as oscillations of the protons and neutrons against each other. In deformed nuclei *(below)* two oscillation modes are available

One can understand these states as a combination of a hole in the remaining nucleus and a particle in a higher shell, and the interaction between the particle and all the nucleons of the now incomplete shell may be viewed as an interaction between the particle and the hole. This interaction depends upon the spin and isospin of the particle-hole system and causes the states to mix strongly. Below we want to use a greatly simplified model to show how the transition strengths of all one particle-one hole states combine through this mixing into a single state.

We use $\mathcal{H}_0$ to denote the Hamiltonian operator of a nucleon in the central potential of the single-particle shell model. In the transition of the particle from a full shell to the one above, we must also take the particle-hole interaction into account; the Hamiltonian operator must then be written as

$$\mathcal{H} = \mathcal{H}_0 + \mathcal{V} . \tag{19.21}$$

Collective excitations appear just because of the mixing generated by this particle-hole interaction $\mathcal{V}$.

Consider now all particle-hole states with 1^- spin and parity. These can only be particle-hole combinations such that the angular momenta $\boldsymbol{j}_1$ and $\boldsymbol{j}_2$ add vectorially to $1\hbar$ and the sum of the orbital angular momentum quantum numbers $\ell_1 + \ell_2$ is odd (so that the parity is negative). If we restrict ourselves to the excitation of a nucleon from the 1p into the 1d or 2s shell, then we have the following possible particle-hole states:

$$\left|\phi^{-1}_{1p_{3/2}}\phi_{1d_{5/2}}\right\rangle, \left|\phi^{-1}_{1p_{3/2}}\phi_{2s_{1/2}}\right\rangle, \left|\phi^{-1}_{1p_{3/2}}\phi_{1d_{3/2}}\right\rangle,$$
$$\left|\phi^{-1}_{1p_{1/2}}\phi_{2s_{1/2}}\right\rangle, \left|\phi^{-1}_{1p_{1/2}}\phi_{1d_{3/2}}\right\rangle.$$

Since both the proton and neutron shells are full in the ^{16}O nucleus, such states exist for both proton and neutron excitations. They have all got roughly the same energy and may be viewed as approximately degenerate.

The number of nucleons per shell is larger in heavy nuclei, and the number of nearly degenerate particle-hole $J^P = 1^-$ states is accordingly greater. The number of particle-hole states, N, is between 10 to 20 for medium-sized nuclei.

The connection between one-particle and collective excitation can be clarified by a simple model [4]. We denote particle-hole states by $|\psi_i\rangle$:

$$|\psi_i\rangle = \left|\phi^{-1}_{j_1}\phi_{j_2}\right\rangle, \qquad \text{where } i = 1 \ldots N . \tag{19.22}$$

The $|\psi_i\rangle$ are, by definition, eigenstates of the unperturbed Hamiltonian

$$\mathcal{H}_0 |\psi_i\rangle = E_i |\psi_i\rangle . \tag{19.23}$$

The solution to the Schrödinger equation with the full Hamiltonian operator

$$\mathcal{H}\,|\Psi\rangle = (\mathcal{H}_0 + \mathcal{V})\,|\Psi\rangle = E\,|\Psi\rangle\,, \tag{19.24}$$

is $|\Psi\rangle$. This wave function $|\Psi\rangle$ projected out upon the space spanned by $|\psi_i\rangle$ in (19.22) may be written as

$$|\Psi\rangle = \sum_{i=1}^{N} c_i\,|\psi_i\rangle\,, \tag{19.25}$$

where the coefficients c_i fulfil the secular equation

$$\begin{pmatrix} E_1 + V_{11} & V_{12} & V_{13} & \cdots \\ V_{21} & E_2 + V_{22} & V_{23} & \cdots \\ V_{31} & V_{32} & E_3 + V_{33} & \cdots \\ \vdots & \vdots & \vdots & \ddots \end{pmatrix} \cdot \begin{pmatrix} c_1 \\ c_2 \\ c_3 \\ \vdots \end{pmatrix} = E \cdot \begin{pmatrix} c_1 \\ c_2 \\ c_3 \\ \vdots \end{pmatrix}. \tag{19.26}$$

We assume for simplicity that all the V_{ij} are the same

$$\langle\psi_i|V|\psi_j\rangle = V_{ij} = V_0\,. \tag{19.27}$$

The solution of the secular equation is then rather simple: the coefficients c_i may be written as

$$c_i = \frac{V_0}{E - E_i} \sum_{j=1}^{N} c_j\,, \tag{19.28}$$

where $\sum_j c_j$ is a constant. Summing over all N particle-hole states on both sides and bearing in mind that $\sum_i c_i = \sum_j c_j$, we obtain the relation

$$1 = \sum_{i=1}^{N} \frac{V_0}{E - E_i}\,, \tag{19.29}$$

as the solution of the secular equation.

The solutions of this equation are most easily understood graphically (Fig. 19.5). The right-hand side of the equation has poles at $E = E_i$ where $i = 1 \ldots N$. The solutions E_i' to (19.29) are to be found where the right-hand side is unity. The new energies are marked by circles on the abscissa; $N-1$ eigenvalues (3 in the diagram) are "squeezed in" between the unperturbed energies $E_1 \ldots E_n$. The exception, denoted by E_C, is the collective state, as we will show in the following. A repulsive ($V_0 > 0$) interaction, as is assumed in the diagram, has its collective state above the particle-hole state.

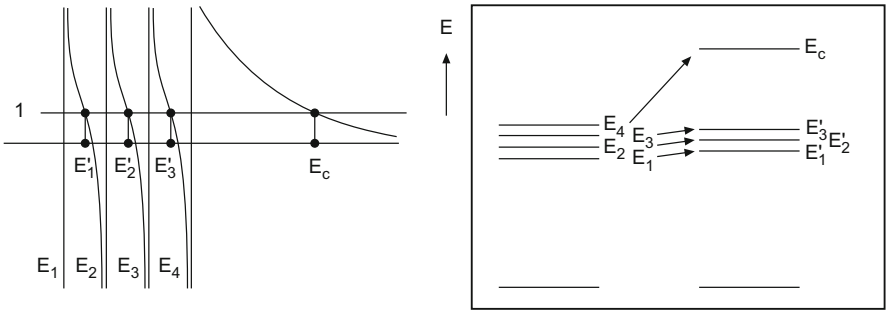

Fig. 19.5 Graphical representation of the solution to the secular equation (19.26) and a picture of how the energy levels are shifted

To obtain a quantitative estimate of the energy shift, we now assume that $E_i = E_0$ for all i. Equation (19.29) then becomes

$$1 = \sum_{i=1}^{N} \frac{V_0}{E_\mathrm{C} - E_i} = \frac{NV_0}{E_\mathrm{C} - E_0}\,, \tag{19.30}$$

from which

$$E_\mathrm{C} = E_0 + N \cdot V_0 \tag{19.31}$$

follows. The energy shift of the collective state is proportional to the number of degenerate states. From experiment we know that the energy of the giant resonance is roughly twice the separation between two shells, i.e., $NV_0 \approx E_0$. The effective interaction decreases for heavier nuclei but this is compensated by the increased number of states which can enter the collective motion.

The expansion coefficients for the collective state

$$c_i^{(\mathrm{C})} = \frac{V_0}{E_\mathrm{C} - E_i} \sum_j c_j^{(\mathrm{C})} \tag{19.32}$$

are nearly independent of i so long as the energy of the collective state E_C is well separated from the E_i. The collective state has the following configuration:

$$|\psi_\mathrm{C}\rangle = \frac{1}{\sqrt{N}} \sum_{j_i j_k} \left| \phi_{j_i}^{-1} \phi_{j_k} \right\rangle . \tag{19.33}$$

This state is singled out by the fact that the amplitudes of each and every particle-hole state add with the same sign (constructively), since $E_\mathrm{C} > E_i$ for all i. For the other $N - 1$ diagonal states only one of the c_j is large and the others are small and have different signs. The superposition of the amplitudes is therefore destructive.

The coherent superposition of the amplitudes means that the transition probability is large for the collective case and otherwise small as we will show in what follows.

If we do not assume as in (19.27) that all the V_{ij} are equal, then the calculation becomes more tedious but the general conclusion remains the same: as long as the V_{ij} are of the same order of magnitude the highest state is shifted well above the others and manifests itself as a coherent sum of all the particle-hole states.

Estimating the transition probability The operator for the electric dipole transition is

$$\boldsymbol{D} = e \sum_{p=1}^{Z} \boldsymbol{x}_p \,, \tag{19.34}$$

where $\boldsymbol{x}_p$ is the coordinate of a proton. This must be modified slightly, since it is not yet clear which coordinate system $\boldsymbol{x}_p$ refers to. The most natural coordinate system is the centre-of-mass system and we therefore write

$$\boldsymbol{D} = e \sum_{p=1}^{Z} \left(\boldsymbol{x}_p - \boldsymbol{X}\right), \qquad \text{where} \qquad \boldsymbol{X} = \frac{1}{A}\left(\sum_{p=1}^{Z} \boldsymbol{x}_p + \sum_{n=1}^{N} \boldsymbol{x}_n\right). \tag{19.35}$$

This may be recast as

$$\boldsymbol{D} = e\frac{N}{A} \sum_{p=1}^{Z} \boldsymbol{x}_p - e\frac{Z}{A} \sum_{n=1}^{N} \boldsymbol{x}_n \,. \tag{19.36}$$

We interpret this expression as meaning that

$$\begin{aligned} e_{\mathrm{p}} &= +eN/A \text{ is the effective proton charge} \quad \text{and} \\ e_{\mathrm{n}} &= -eZ/A \text{ is the effective neutron charge.} \end{aligned} \tag{19.37}$$

A photon "pulls" the protons in one direction and the neutrons in the opposite one. The neutrons and protons always move oppositely to each other under the influence of the photon in such a way that the centre-of-mass stays in the same place.

If we replace ψ_i and ψ_f in (19.1) by the nucleon wave functions in the one-particle shell model before and after the γ emission, we find the so-called one-particle transition probability. This, weighted with the square of the effective charge, may be used to estimate the collective nature of transitions.

We need to use the wave function (19.33) to calculate the matrix element

$$\mathcal{M}_{fi} = \int \mathrm{d}^3x \; \psi_f^* \, D_z \, \psi_i \;, \tag{19.38}$$

where D_z is the z component of the dipole operator (19.34), if we want to calculate the transition probability. In our case ψ_i is just $|0\rangle$, the wave function of the ground state with closed shells and ψ_f is the wave function (19.33) of the collective excitation. Thus we have

$$\mathcal{M}_{C0} = \frac{1}{\sqrt{N}} \int \mathrm{d}^3x \left\{ \left\langle \phi_{j_i}^{-1} \phi_{j_k} \right| + \left\langle \phi_{j_l}^{-1} \phi_{j_m} \right| + \ldots \right\} D_z \, |0\rangle \, . \tag{19.39}$$

The matrix element between the ground state and the particle-hole excitation can be identified with the dipole transition of a particle from a closed shell into a higher one. The integrals

$$A_n \;=\; \int \mathrm{d}^3x \, \phi_{j_k}^* D_z \phi_{j_i} \tag{19.40}$$

represent the amplitude for the transition of a particle from the j_i shell into the j_k one. Here n is an index which denotes each of the total N particle-hole states. The phases of the transition amplitudes A_n that contribute to the collective state are the phases of the differences of the magnetic substates. In the square of the amplitudes an equal number of mixed terms with positive and negative signs occur; they therefore average out to zero. If we assume for simplicity that the moduli $|A_n|$ are also identical, then the squared matrix element becomes

$$|\mathcal{M}_{C0}|^2 \;=\; \frac{1}{N} \left| \sum_{n=1}^{N} A_n \right|^2 \;=\; \frac{N^2}{N} \, |A|^2 \;=\; N \left| M_{\text{1-particle}} \right|^2 . \tag{19.41}$$

The transition probabilities are then rearranged. Because the states mix, we no longer have N different states each excited with probability $|A|^2$, but rather the total transition probability $N|A|^2$ is taken up by the collective state.

These ideas apply equally to both protons and neutrons. But, since the proton and neutron effective charges (19.37) are of opposite signs, protons and neutrons oscillate inside the nucleus with opposite phases. This is the semiclassical interpretation of the giant dipole resonance.[1] The oscillation in deformed nuclei can take place along or orthogonal to the symmetry axis. This leads to two peaks in the excitation curve, as is seen in Fig. 19.3 for the case of ^{150}Nd.

This treatment of the collective dipole resonance in a shell model, where we limited ourselves to just a few particle-hole states and then actually only solved it schematically, explains why the dipole transition strength is essentially restricted to one state. The resonance lies above the neutron threshold, i.e., in the continuum, and primarily mixes with neutron scattering states. Thus the cross-section for photon absorption displays a broad structure instead of a narrow state.

[1] There is an attractive analogy to the giant dipole resonance in plasma physics: electromagnetic radiation directed at a plasma is absorbed over a broad band around the so-called plasma frequency. At this frequency the totality of the free electrons oscillate against the ions.

19.3 Shape Oscillations

Quadrupole oscillations Other nuclear collective states have also been observed in experiments. To keep things simple, we will limit ourselves in what follows to doubly even nuclei. Their ground and first excited states always have quantum numbers $J^P = 0^+$ and $J^P = 2^+$, with the exception of doubly magic nuclei and a very few others (Figs. 18.6 and 19.6). The simplest explanation for these excited levels would be that a nucleon pair has been broken apart to produce the second lowest energy level, $J^P = 2^+$. Measurements of the lifetimes of such states show, however, that the transition probability for the electric quadrupole transition is up to two orders of magnitude larger than a one-particle transition would suggest. The lowest 2^+ states are in fact, for nuclei with enough particles outside closed shells, our first encounter with the ground-state rotational band which we will treat in Sect. 19.4. If the configuration has only a few particles outside closed shells, then we describe these states as oscillations of the geometric shape of the nucleus around its equilibrium form, which last is approximately spherically symmetric. For such 2^+ states it seems likely that these vibrations are of the quadrupole type (Fig. 19.7a).

Near the giant dipole resonance, and so at much higher excitation energies, further collective states with $J^P = 2^+$ are observed in electron scattering. These are called giant quadrupole resonances.

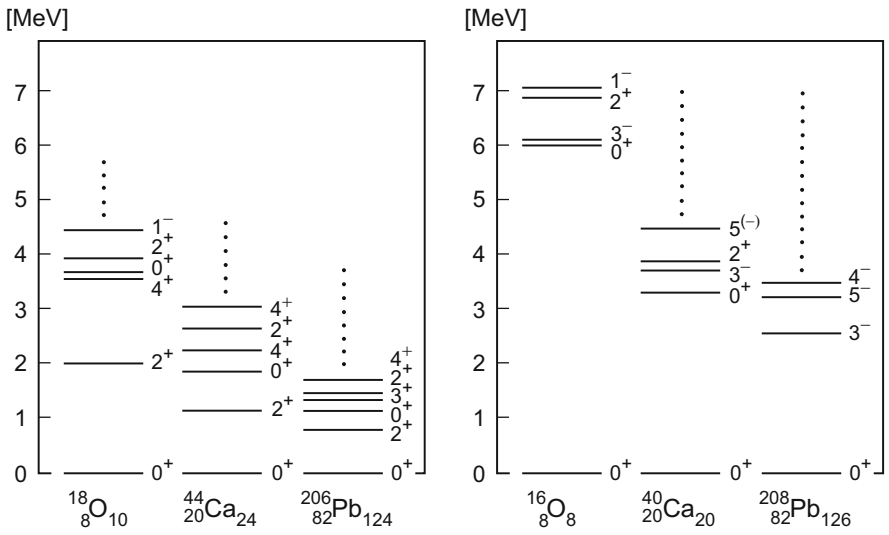

Fig. 19.6 Energy levels of three simply magic even-even nuclei, ^{18}O, ^{44}Ca and ^{206}Pb (*left*), and three doubly magic ones, ^{16}O, ^{40}Ca and ^{208}Pb (*right*). The excited states in the first case have $J^P = 2^+$. This state is lacking in the three doubly magic nuclei, which instead have a lower lying 3^- state. The transition probability into the ground state is high compared with what we would expect from a single-particle excitation. These states are interpreted as collective quadrupole or octupole vibrations

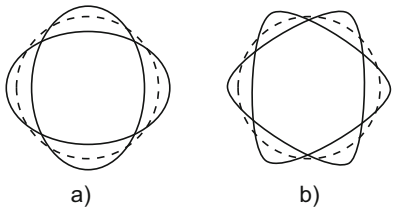

Fig. 19.7 (**a**) Quadrupole vibrations; (**b**) Octupole vibrations

This illustrative discussion of quadrupole oscillations needs to be explained, in a similar fashion to our treatment of the giant dipole resonance, in terms of the shell model and the nature of the nuclear force. In a single-particle picture collective excitations only arise if the particles in a shell are excited with correlated phases. For the giant dipole resonances we saw that this took place through coherent addition of all particle-hole excitations. To now create $J^P = 2^+$ states we need to either promote one particle into the next but one shell, or into the next level inside the same shell. This is a consequence of the spin and parity of the shell states. Shells below ^{48}Ca have alternating $+1$ and -1 parity and in heavier nuclei at least states with similar j will have opposite parities in successive shells. The particle-hole states are in this case nearly degenerate which can lead to collective states. Exciting particles inside the same shell leads to low lying quadrupole vibrations, exciting them into the next but one shell generates giant quadrupole resonances.

While the semiclassical picture of a giant dipole resonance has the protons and neutrons oscillating against each other, the protons and neutrons in nuclear quadrupole oscillations can move either with the same or opposite phase. If they move in phase the isospin is unchanged, if oppositely it is changed by unity. We will only consider the first case here. The interaction between particle-hole states which causes this in-phase motion is, obviously, of an attractive type. If we were to solve the secular equation for a collective 2^+ state, we would see that the attractive interaction shifts the energy levels downwards. The lowest energy state is built up out of a coherent superposition of particle-hole states with $J^P = 2^+$ and is collectively shifted down.

The various collective excitations in the framework of the shell model are depicted in Fig. 19.8. The giant quadrupole resonance splits into two parts. That with $\Delta I = 1$, which comes from proton-neutron repulsion, is, similarly to the giant dipole resonance, shifted up to higher energies. The giant quadrupole resonance which has $\Delta I = 0$ corresponds to shape oscillations and is shifted down. In both cases, however, the shift is smaller than was the case for the giant dipole resonance, which implies that the collective nature of these excitations is less pronounced. This may be explained as follows: the one-particle-one-hole excitations which build up the giant dipole resonance can only, for reasons of energy, enter a few other states, which themselves are one-particle-one-hole excitations in the same shell combinations. This state made up of single-particle-hole excitations is thus long lived and displays a strongly coherent nature. This is all no longer true for excitations into the next shell but one, such as those which comprise the quadrupole

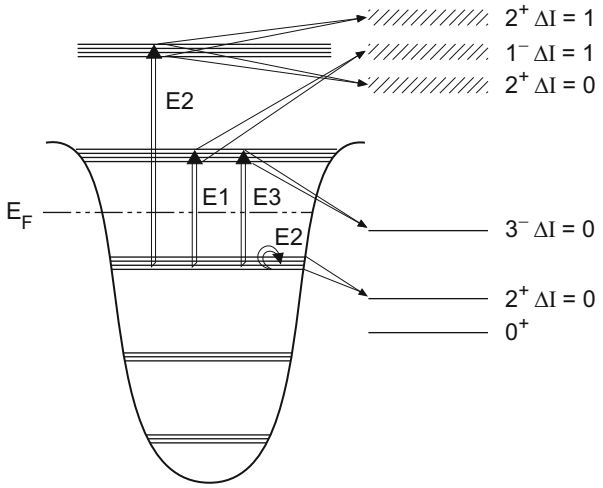

Fig. 19.8 Collective excitations in the framework of the shell model. Shape oscillations are denoted by $\Delta I = 0$. Those collective states where the protons and neutrons oscillate in phase are shifted downwards. States where they oscillate with opposite phases ($\Delta I = 1$) are pushed up to higher energies. Shells below the Fermi energy E_F are occupied by nucleons. The ground state lies at a position below the single-particle excitations given by the pairing energy

resonance. The single-particle-hole excitations of the next shell but one can decay into two-particle-hole states. Hence they have shorter lifetimes, are less coherent and less collective.

If the protons and neutrons move in phase this appears as a change in the shape of the nucleus. This alteration can hardly be quantitatively described in the shell model, since its particle wave functions were obtained using a spherically symmetric potential. Shape oscillations change the form of the potential and the nucleonic motion has to alter itself accordingly. Quantitative treatments of nuclei with large quadrupole oscillations are then of a hybrid form, where the total wave function has both vibrational and single-particle parts.

Octupole oscillations Nuclei with doubly closed shells, like ^{16}O, ^{40}Ca and ^{208}Pb, possess a low-lying 3^- state (Fig. 19.6) whose transition probability can be up to two orders of magnitude higher than the single-particle prediction. This state can be interpreted as an octupole vibration (Fig. 19.7b). The collective 3^- states can, like the giant dipole resonance, be built up out of particle-hole excitations in neighbouring shells. Since the protons and neutrons oscillate in phase in such shape vibrations, the particle-hole interaction must be attractive. The collective octupole excitations are shifted to lower energies.

Summary The picture of collective excitations which we have here attempted to explain is the following: since the shell energies in the nucleus are distinctly separated from each other, those particle-hole states which are created when a

nucleon is excited into a higher shell are nearly degenerate. Coherent superposition of these particle-hole states then form a collective excitation. Shape oscillations can be interpreted as coherent superpositions of the movement of single particles, but a quantitative description is only possible in terms of collective variables.

19.4 Rotational States

Nuclei with sufficiently many nucleons outside of closed shells display a characteristic excitation pattern: a series of states with increasing total angular momentum, the separation between whose energies increases linearly. These excitations are interpreted as corresponding to the nucleus rotating and, in analogy to molecular physics, the series are called *rotational bands*. Electric quadrupole transitions between the states of a rotational band display a markedly collective nature. The excitation pattern, and also the collective character of the quadrupole transitions, are understood as consequences of these nuclei being highly deformed [3]. Generally speaking the spin of the nuclear ground state is coupled to the angular momentum of the collective excitations. We will bypass this complication by only considering even-even nuclei, since these have spin zero in the ground state.

Rotational energy in classical mechanics depends upon the angular momentum $\boldsymbol{J}$ and the moment of inertia Θ:

$$E_{\text{rot}} = \frac{|\boldsymbol{J}_{\text{rot}}|^2}{2\Theta} \,. \tag{19.42}$$

In quantum mechanics rotation is described by a Hamiltonian operator

$$\mathcal{H}_{\text{rot}} = \frac{\boldsymbol{J}^2}{2\Theta} \,. \tag{19.43}$$

In such a quantum mechanical system the rotation must be perpendicular to the symmetry axis. The eigenstates of the angular momentum operator $\boldsymbol{J}$ are the spherical harmonic functions Y_J^m, which describe the angular distribution of the wave function. The associated eigenvalues are:

$$E_J = J(J+1)\frac{\hbar^2}{2\Theta} \,. \tag{19.44}$$

The gaps between successive states increase linearly because of $E_{J+1} - E_J = 2(J+1)\hbar^2/2\Theta$. This is typical of rotating states. Only even values of J are attainable, for reasons of symmetry, for those nuclei which have $J^P = 0^+$ in the ground state. The moment of inertia Θ can be found from the spins and excitation energies.

We want to discuss the experimental data through two examples which we have chosen out of the range of masses where highly deformed nuclei occur: the lanthanides and the actinides.

Coulomb excitation Coulomb excitations in heavy ion reactions are often used to produce highly excited rotating states. To ensure that the interaction only takes place via Coulomb excitation, both partners must remain further apart than the range of the nuclear force. The projectile energy must then be chosen such that the *Coulomb threshold*

$$E_{\mathrm{C}} = \frac{Z_1 Z_2 e^2}{4\pi\varepsilon_0} \frac{1}{R_1 + R_2} = \frac{Z_1 Z_2 \alpha \cdot \hbar c}{R_1 + R_2} \tag{19.45}$$

of the partners is not crossed. Larger values for the radii R_1 and R_2 of the reacting particles than in (5.56), say $R = 1.68\ \mathrm{fm} \cdot A^{1/3}$ are then assumed to make sure that the tails of the nuclear wave functions do not have any effects [5].

Consider now the example of the Coulomb scattering of a $^{90}_{40}$Zr projectile off a $^{232}_{90}$Th target nucleus. The ^{90}Zr ion is accelerated in a Tandem Van de Graaff accelerator up to a kinetic energy of $E_{\mathrm{Zr}} = 415\,\mathrm{MeV}$. The centre-of-mass energy which is then available to the colliding particles is

$$E_{\mathrm{cm}} = \frac{A_{\mathrm{Th}}}{A_{\mathrm{Zr}} + A_{\mathrm{Th}}} E_{\mathrm{Zr}} \approx 299\,\mathrm{MeV}\,. \tag{19.46}$$

If we insert the charge numbers and radii of these two nuclei into (19.45), we find that $E_{\mathrm{C}} \approx 300\,\mathrm{MeV}$. The centre-of-mass energy is, in other words, just below the limit where the first non-electromagnetic effects would make themselves felt.

The ^{90}Zr projectile nucleus follows a hyperbolic path in the field of the target nucleus (Fig. 19.9a) and exposes the ^{232}Th nucleus to a rapidly changing electric field. The path of the ion is so sharply curved that frequencies in the time-dependent electric field are generated that are high enough to produce individual excitations with energies up to about 1 MeV.

There is not just a quantitative but also a qualitative difference between Coulomb excitation and electron scattering off nuclei:

- The principal distinction is that the interaction is much stronger with a projectile charge which is Z times that of the electron. One must replace α by $Z\alpha$ in the matrix element (5.31). This means that the cross-section increases as Z^2.
- If we are not to cross the Coulomb threshold, the projectile energy must be so low that its velocity obeys $v \lesssim 0.05\,c$. Magnetic forces are hence of little importance.
- The ion orbit may be calculated classically, even for inelastic collisions. The kinetic energy of the projectile in Coulomb excitation changes by less than 1 % and thus its path is practically the same. The frequency distribution of the virtual photons is very well known and the transition amplitudes can be worked out to a high degree of accuracy.

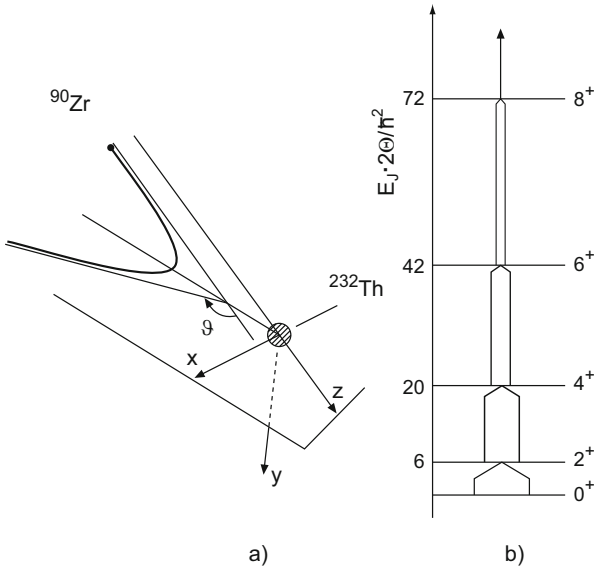

Fig. 19.9 (**a**) Kinematics of a heavy ion collision (here ^{90}Zr + ^{232}Th). The projectile follows a hyperbolic orbit in the Coulomb field of the target nucleus. (**b**) Sketch of multiple Coulomb excitation of a rotational band. Successive quadrupole excitations lead to the $2^+, 4^+, 6^+, 8^+, \ldots$ states being populated (with decreasing intensity)

The large coupling strength means that successive excitation from one level to the next is now possible. This is sketched in Fig. 19.9b: the quadrupole excitation reproduces itself inside a rotational band from the 2^+ state via the 4^+ to the 6^+.

The popularity of Coulomb excitation in gamma spectroscopy is well founded. In such reactions we primarily produce states inside rotational bands. The cross-sections into the excited states give us, through the transition probabilities, the most important information about the collective nature of the rotational bands. Measurements of the cross-sections into the various states simultaneously determine the transition probability for the electric quadrupole transition inside the rotational band.

The introduction of germanium semiconductor detectors has marked a very significant step forward in nuclear-gamma spectroscopy. The low energy part of the gamma spectrum of Coulomb excitation of ^{232}Th from scattering with ^{90}Zr ions is shown in Fig. 19.10. This gamma spectrum was recorded with a Ge-semiconductor counter and a coincidence condition for the backwardly scattered ^{90}Zr ions, which were measured with a Si-semiconductor detector (Fig. 19.11).

Excellent energy resolution makes it possible to see individual transitions inside rotational bands. Three series of lines can be recognised. The strongest are transitions inside the ground state rotational band ($J_g \rightarrow (J-2)_g$). According to (19.42) these lines should be equidistantly spaced out. This is only approximately the case. This may be explained by noting that the moment of inertia increases with

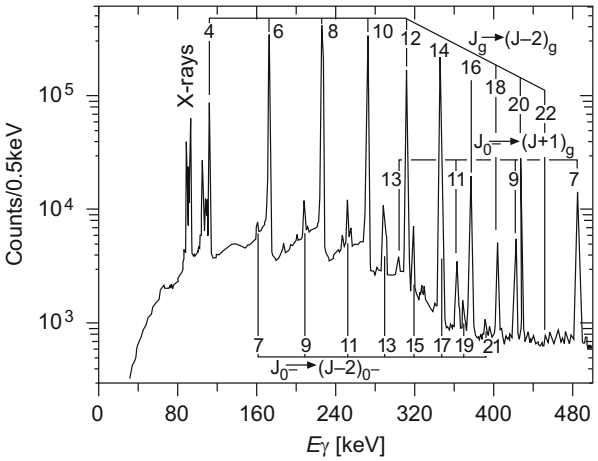

Fig. 19.10 Photon spectrum of a Coulomb excited ^{232}Th nucleus. Three series of matching lines may be seen. The strongest lines correspond to transitions in the ground state rotational band $J_g \rightarrow (J-2)_g$. The other two bands are strongly suppressed and are the results of excited states (cf. Fig. 19.12) [8]

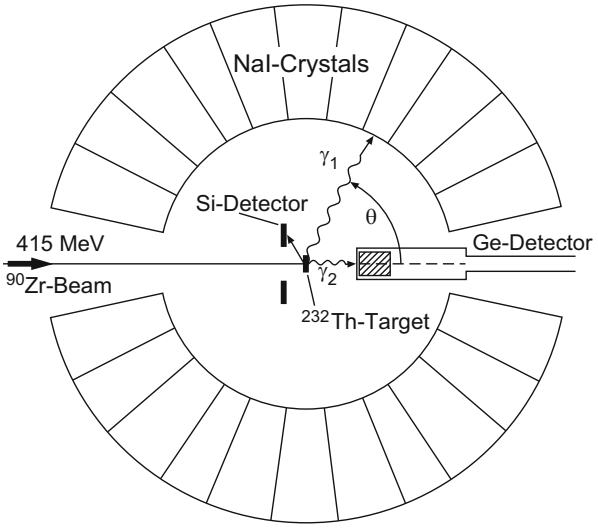

Fig. 19.11 Experimental apparatus for investigating Coulomb excitation in heavy ion collisions. In the example shown a ^{90}Zr beam hits a ^{232}Th target. The backwardly scattered Zr projectiles are detected in a silicon detector. A germanium detector, with which the γ cascades inside the rotational bands can be finely resolved, gives a precise measurement of the γ spectrum. These photons are additionally measured by a crystal ball of NaI crystals with a poorer resolution. A coincidence condition between the silicon detector and the NaI crystals can be used to single out an energy window inside which one may study the nuclear rotational states with the germanium detector (From [8])

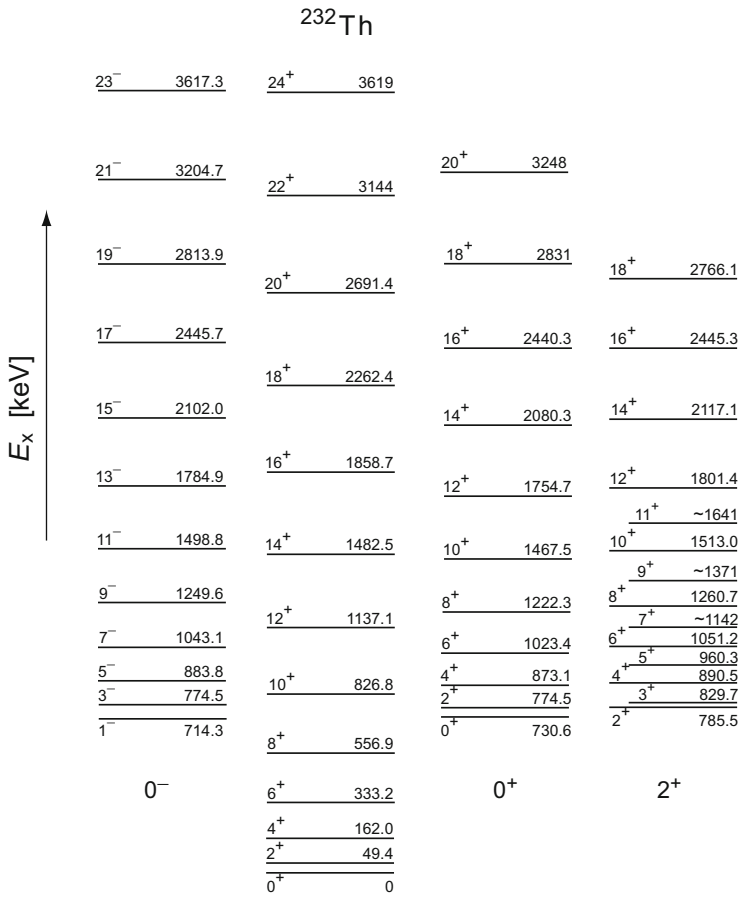

Fig. 19.12 Spectrum of the ^{232}Th nucleus. The excitation energies are in keV. As well as the ground state rotational band, which may be excited up to $J^P = 24^+$, other rotational bands have been observed which are built upon vibrational excitations (From [8]). The quantum numbers of the vibrational states are given below the bands. For reasons of symmetry, the only rotational states which can be constructed upon the $J^P = 0^-$ vibrational state are those with odd angular momenta

the spin. Events with scattering angles around 180° are chosen because the projectile must then have gotten very close to the target and at the moment of closest approach have experienced a strong acceleration. The virtual-photon spectrum which the projectile emits contains high frequencies which are important for the excitation of the high spin states. The spectrum which emerges from this sort of measurement is shown in Fig. 19.12: as well as the ground state rotational band, there are other rotational bands which are built upon excited states. In this case the excitations may be understood as vibrational states.

Fusion reactions Records in high spin excitations may be obtained with the help of fusion reactions such as

$$^{48}\mathrm{Ca} + {}^{108}\mathrm{Pd} \longrightarrow {}^{156}\mathrm{Dy} \longrightarrow {}^{152}\mathrm{Dy} + 4\,\mathrm{n}\,.$$

Only ^{48}Ca nuclei with a kinetic energy of 200 MeV can just overcome the Coulomb barrier. If the fusion process takes place when the nuclei just touch, then the ^{156}Dy fusion product receives angular momentum

$$\ell\hbar \approx (R_1 + R_2)\sqrt{2mE}\,, \tag{19.47}$$

where m is the reduced mass of the ^{48}Ca-^{108}Pd system; R_1 and R_2 are of course the correct nuclear radii from (5.56). The calculation thus yields $\ell \approx 180$. In practice the fusion reaction only takes place if the projectile and target overlap, so this number should be understood as an upper limit on the accessible angular momentum. Experimentally states up to $J^P = 60^+$ have been reached in this reaction (Fig. 19.14).

The moment of inertia The size of the moment of inertia can with the aid of (19.44) be extracted from the measured energy levels of the rotational bands. The deformation ε can be obtained from the transition probability for electric quadrupole radiation inside the rotational band. The matrix element for the quadrupole radiation is proportional to the quadrupole moment of the nucleus, which, for collective states, is given by (18.40). The observed connection between the moment of inertia and the deformation parameter is displayed in Fig. 19.13. Note that the nuclear moments of

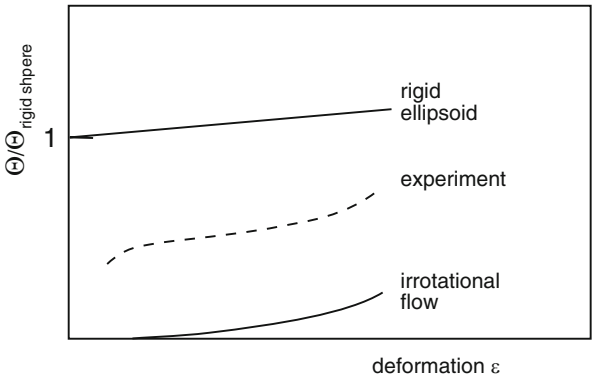

Fig. 19.13 Moments of inertia of deformed nuclei compared with a rigid sphere as a function of the deformation parameter ε. The extreme cases of a rigid ellipsoid and an irrotational liquid are given for comparison

inertia are normalised to those of a rigid sphere with radius R_0

$$\Theta_{\text{rigid sphere}} = \frac{2}{5} M R_0^2 \,. \tag{19.48}$$

The moment of inertia increases with the deformation and is about half that of a rigid sphere.[2]

Two extreme cases are also shown in Fig. 19.13. The moment of inertia is maximised if the deformed nucleus behaves like a rigid body. In this case we have (for small deformations ε) $\Theta \approx (1 + \varepsilon/2) \cdot \Theta_{\text{rigid sphere}}$.

The other limit is reached if the nucleus behaves like an irrotational liquid. Superfluid ^{4}He is an example of an ideal fluid, incompressible and frictionless. Currents in a frictionless liquid are irrotational. A rotating massless eggshell filled with superfluid helium would have the moment of inertia of an irrotational current. Only the bulge of the egg, and not the interior, would contribute to the moment of inertia. The moment of inertia for such an object is

$$\Theta = \frac{405\varepsilon^2}{64\pi} \cdot \Theta_{\text{rigid sphere}} \,, \tag{19.49}$$

where ε is the deformation parameter from (18.39).

Let us return to the example of the ^{232}Th nucleus. The transition probabilities yield a deformation parameter of $\varepsilon = 0.17$. If the rotation of the nucleus could be described as that of an irrotational current, then its moment of inertia would, from (19.49), have to be 6 % of that of a rigid sphere. The level spacings of the ground-state band yield, however

$$\frac{\Theta_{^{232}\text{Th}}}{\Theta_{\text{rigid sphere}}} \approx 0.3 \,. \tag{19.50}$$

This implies that the experimentally determined moment of inertia lies between the two extremes (Fig. 19.13).

This result may be understood at a qualitative level rather easily. We mentioned in Sect. 18.4 that nuclear deformation is a consequence of an accumulation of mutually attractive orbitals either parallel to the symmetry axis (prolate shape) or perpendicular to it (oblate shape). The deformation is associated with the orbitals and one would expect deformed nuclei to rotate like rigid ellipsoids; but this clearly does not happen. This deviation from the rotation of a rigid rotator implies that nuclear matter must have a superfluid component. Indeed nuclei behave like eggshells that are filled with a mixture of a normal fluid and a superfluid.

[2]The comparison with a rigid sphere is, of course, purely classical; a spherically symmetric quantum mechanical system cannot rotate.

The superfluid components of nuclear matter are presumably generated by the pairing force. Nucleons with opposite angular momenta combine to form pairs with spin zero (cf. p. 322). Such zero spin systems are spherically symmetric and cannot contribute to the rotation. The pair formation may be understood analogously to the binding of electrons in *Cooper pairs* in superconductors [1, 6]. The paired nucleons represent, at least as far as rotation is concerned, the superfluid component of nuclear matter. This means on the other hand that not all nucleons can be paired off in deformed nuclei; the larger the deformation, the more nucleons must remain unpaired. This explains why the moment of inertia increases with the deformation (Fig. 19.13).

A similar dependence of the moment of inertia upon the unpaired nucleons can be seen in the rotational bands. The speed of rotation of the nucleus, and hence the centrifugal force upon the nucleons, increases with angular momentum. This causes nucleon pairs to break apart. Thus for large angular momenta the moment of inertia approaches that of a rigid rotator, as one can vividly demonstrate in ^{152}Dy.

The excitation spectrum of ^{152}Dy (Fig. 19.14) is more than a little exotic. The ground state of ^{152}Dy is not strongly deformed, as one sees from the fact that the levels in the ground state rotational band do not strictly follow the $E \propto J(J+1)$ law and that transition probabilities are small. This band, in which the 0^+ until 46^+ states have been observed, first shows a genuine rotational character for high spins. The band which goes up to $J^P = 60^+$ is particularly interesting [12]. The moment of inertia of this band is that of a rigid ellipsoid whose axes have the ratios $2:1:1$ [9]. The transition probabilities inside this band are of the order of 2000 single-particle probabilities. Additionally to these two rotational bands, which have a prolate character, states have been found which may be interpreted as those of an oblately deformed nucleus. Evidently ^{152}Dy has two energy minima near to its ground state, a prolate and an oblate shape. This example shows very nicely that for nuclei with incomplete shells a deformed shape is more stable than a sphere. Tiny changes in the configuration of the nucleus decide whether the prolate or oblate form is energetically favoured (Fig. 18.11).

Further excitations of deformed nuclei We have here only treated the collective aspects of rotation. Generally, however, excitations occur where, as well as rotation, an oscillation around either the equilibrium shape of the deformed nucleus or single-particle excitations are seen. (The latter case may be particularly clearly seen in odd nuclei.) The single-particle excitations may be, as described in Sect. 18.4, calculated from the movement of nucleons in a deformed potential. Deformed nuclei may be described, similarly to their vibrating brethren, in a hybrid model which employs collective variables for the rotational and vibrational degrees of freedom. The single-particle motion is coupled to these collective variables. The names of Bohr and Mottelson in particular are associated with the work that showed that a consistent description of nuclear excitations is possible in such hybrid models.

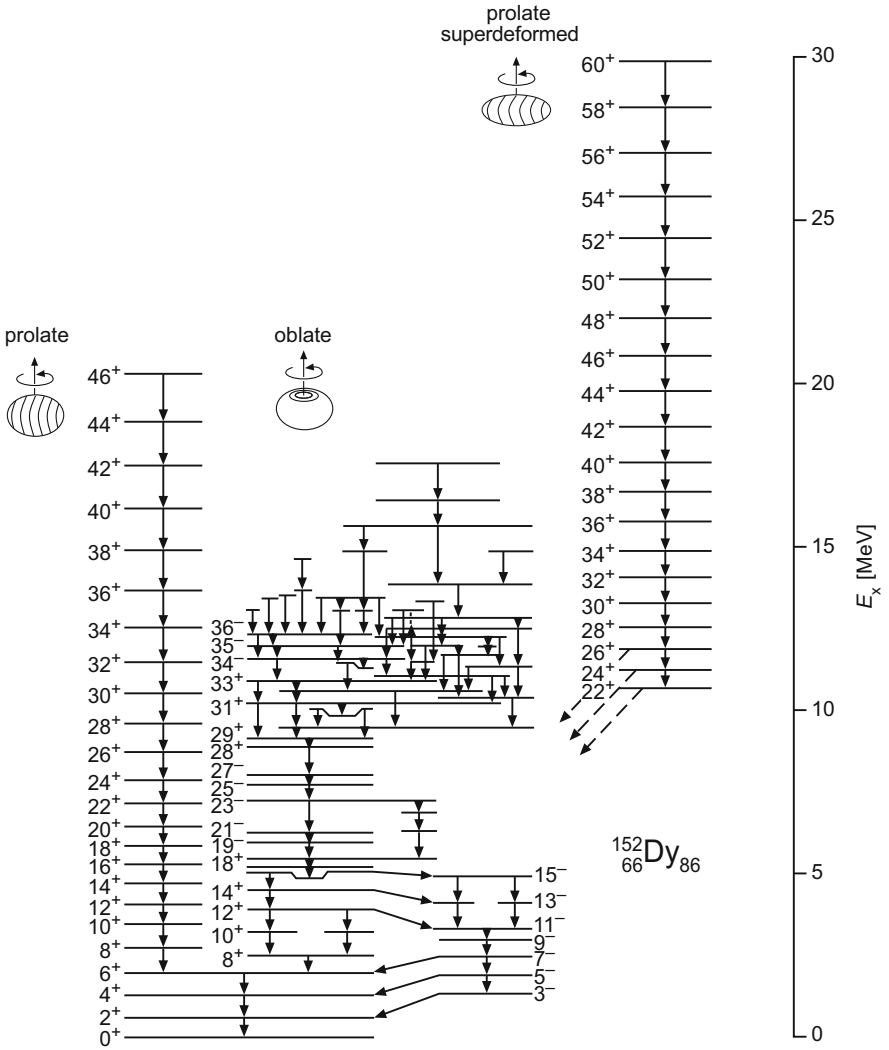

Fig. 19.14 Energy levels of ^{152}Dy [11]. Although the low energy levels do not display typical rotational bands, these are seen in the higher excitations, which implies that the nucleus is then highly deformed

Problems

1. **The electric dipole giant resonance**

   (a) How large is the average deviation between the centres-of-mass of the protons and neutrons in giant dipole resonances for nuclei with $Z = N = A/2$?

The A dependence of the resonance energy is very well described by $\hbar\omega \approx 80\,\mathrm{MeV}/A^{1/3}$. Give the numerical value for ^{40}Ca.

(b) Calculate the squared matrix element for the dipole transition in this model.

(c) Calculate the matrix element for a proton or neutron dipole transition (19.36) in the shell model with a harmonic oscillator potential. Use the fact that single particle excitations are about half the size of those of the giant resonance.

2. **Deformation**
   The deformation parameter of the $^{176}{}_{71}$Lu nucleus is $\varepsilon = +0.21$. Find the semi-axes a and b of the rotational ellipsoid, describe its shape and calculate the quadrupole moment of this nucleus.
3. **Rotational bands**
   The rotational band of ^{152}Dy in Fig. 19.14 which extends up to $J^P = 60^+$ corresponds to the rotation of an ellipsoid the ratio of whose axes is $2:1:1$. What would be the velocity of the nucleons at the "tip" of the ellipsoid if this was a rotating rigid body? Compare this velocity with the *average* speed of nucleons in a Fermi gas with $p = p_\mathrm{F} = 250\,\mathrm{MeV}/c$.

References

1. J. Bardeen, L.N. Cooper, J.R. Schrieffer, Phys. Rev. **108**, 1157 (1957)
2. B.L. Berman, S.C. Fultz, Rev. Mod. Phys. **47**, 713 (1975)
3. A. Bohr, B.R. Mottelson, Mat. Fys. Medd. Dan. Vid. Selsk. **27**, no 16 (1953)
4. G.E. Brown, *Unified Theory of Nuclear Models and Forces* (North Holland, Amsterdam, 1967)
5. P.R. Christensen et al., Nucl. Phys. **A207**, 33 (1973)
6. L.N. Cooper, Phys. Rev. **104**, 1186 (1956)
7. E. Fermi, *Nuclear Physics*, 5th edn. (University of Chicago Press, Chicago, 1953)
8. W. Korten, 'Suche nach Mehr - Phonon Banden in 232Th' (in german), Dissertation, Heidelberg (1988)
9. I. Ragnarsson, S. Åberg, Phys. Lett. **B180**, 191 (1986)
10. F. Schwabl, *Quantum Mechanics*, 4th edn. (Springer, Berlin/Heidelberg/New York, 2007)
11. J. Sharpey-Schafer, Phys. World **3**(Nr. 9), 31 (1990)
12. P.J. Twin et al., Phys. Rev. Lett. **57**, 811 (1986)